



**HAL**  
open science

## Prolate-Spherical Shape Coexistence at $N=28$ in $^{44}\text{S}$

C. Force, S. Grévy, L. Gaudefroy, O. Sorlin, L. Caceres, F. Rotaru, J. Mrazek,  
N.L. Achouri, J.C. Angélique, F. Azaiez, et al.

► **To cite this version:**

C. Force, S. Grévy, L. Gaudefroy, O. Sorlin, L. Caceres, et al.. Prolate-Spherical Shape Coexistence at  $N=28$  in  $^{44}\text{S}$ . *Physical Review Letters*, 2010, 105, pp.102501. 10.1103/PhysRevLett.105.102501 . in2p3-00506598

**HAL Id: in2p3-00506598**

**<https://hal.in2p3.fr/in2p3-00506598>**

Submitted on 28 Jul 2010

**HAL** is a multi-disciplinary open access archive for the deposit and dissemination of scientific research documents, whether they are published or not. The documents may come from teaching and research institutions in France or abroad, or from public or private research centers.

L'archive ouverte pluridisciplinaire **HAL**, est destinée au dépôt et à la diffusion de documents scientifiques de niveau recherche, publiés ou non, émanant des établissements d'enseignement et de recherche français ou étrangers, des laboratoires publics ou privés.

## Prolate-Spherical Shape Coexistence at N=28 in $^{44}\text{S}$

C. Force,<sup>1</sup> S. Grévy,<sup>1,\*</sup> L. Gaudefroy,<sup>2</sup> O. Sorlin,<sup>1</sup> L. Caceres,<sup>1</sup> F. Rotaru,<sup>3</sup> J. Mrazek,<sup>4</sup> N. L. Achouri,<sup>5</sup> J. C. Angélique,<sup>5</sup> F. Azaiez,<sup>6</sup> B. Bastin,<sup>5</sup> R. Borcea,<sup>3</sup> A. Buta,<sup>3</sup> J. M. Daugas,<sup>2</sup> Z. Dlouhy,<sup>4</sup> Zs. Dombrádi,<sup>7</sup> F. De Oliveira,<sup>1</sup> F. Negoita,<sup>3</sup> Y. Penionzhkevich,<sup>8</sup> M. G. Saint-Laurent,<sup>1</sup> D. Sohler,<sup>7</sup> M. Stanoiu,<sup>3</sup> I. Stefan,<sup>1</sup> C. Stodel,<sup>1</sup> and F. Nowacki<sup>9</sup>

<sup>1</sup>Grand Accélérateur National d'Ions Lourds (GANIL), CEA/DSM-CNRS/IN2P3, Caen, France

<sup>2</sup>CEA, DAM, DIF, F-91297 Arpajon, France

<sup>3</sup>Institute of Atomic Physics, IFIN-HH, Bucharest-Magurele, P.O. Box MG6, Romania

<sup>4</sup>Nuclear Physics Institute, AS CR, CZ-25068 Rez, Czech Republic

<sup>5</sup>LPC Caen, ENSICAEN, Université de Caen, CNRS/IN2P3, Caen, France

<sup>6</sup>IPNO, Université Paris-Sud 11, CNRS/IN2P3, Orsay, France

<sup>7</sup>Institute of nuclear Research, H-4001 Debrecen, Pf.51, Hungary

<sup>8</sup>FLNR, JINR, 141980 Dubna, Moscow region, Russia

<sup>9</sup>IPHC, CNRS/IN2P3 and Université de Strasbourg, F-67037 Stasbourg Cedex 2, France

(Dated: July 28, 2010)

The structure of  $^{44}\text{S}$  has been studied using delayed  $\gamma$  and electron spectroscopy at GANIL. The decay rates of the  $0_2^+$  isomeric state to the  $2_1^+$  and  $0_1^+$  states have been measured for the first time, leading to a reduced transition probability  $B(E2 : 2_1^+ \rightarrow 0_2^+) = 8.4(26) \text{ e}^2\text{fm}^4$  and a monopole strength  $\rho^2(E0 : 0_2^+ \rightarrow 0_1^+) = 8.7(7) \times 10^{-3}$ . Comparisons to shell model calculations point towards prolate-spherical shape coexistence and a phenomenological two level mixing model is used to extract a weak mixing between the two configurations.

PACS numbers: 23.20.Lv, 25.70.Mn; 27.40.+z, 29.30.Kv

'Magic' nuclei exhibit large gaps between the occupied and valence orbits. They are cornerstones of the nuclear structure, being used (i) to test our understanding of the nuclear forces which form these gaps and (ii) to model more complicated systems having many valence nucleons. While nuclei having 8 and 20 protons (or neutrons) can be reproduced by modeling the atomic nucleus with an harmonic oscillator potential, a spin-orbit interaction must be added to describe heavier magic nuclei. This spin-orbit interaction strongly binds nucleons having their angular momenta  $\ell$  aligned with their intrinsic spin value  $s$ , denoted as  $\ell_\uparrow$ . This leads throughout the chart of nuclei to regular sequence of orbits  $\ell_\uparrow$ ,  $(\ell - 2)_\uparrow$ ,  $(\ell - 2)_\downarrow$ ,  $\ell_\downarrow$ , with the so-called large spin-orbit gaps 14, 28, 50, 82 and 126 between the lowered  $\ell_\uparrow$  orbit ( $\ell=2, 3, 4, 5$  and 6) and the others. Generally, in particular at the stability, these gaps are large enough to prevent excitations between occupied and valence orbits and these magic nuclei are spherical. However, as the orbits forming the gap are separated by two units of angular momentum, quadrupole excitations are likely to develop if for some reason the shell gap is reduced. In this hypothesis, the development of quadrupole excitations jeopardizes the rigidity of the spherical gap and conduct the nucleus to deform. Consequently the doubly magic nuclei which have proton and neutron spin-orbit shell closures could become vulnerable to quadrupole excitations, as both protons and neutrons could act co-

herently to deform the nucleus. So far *the* prototypical deformed nucleus composed of such a double spin-orbit shell-closure is  $^{42}\text{Si}_{28}$  [1]. At N=28 a gradual development of deformation occurs between the spherical doubly magic  $^{48}\text{Ca}_{28}$  and the deformed  $^{42}\text{Si}_{28}$ . In between these two extremes, i.e. in  $^{44}\text{S}_{28}$ , competition between spherical and deformed shapes is expected to be present leading to shape coexistence [2–4]. Depending on the strength of the quadrupole correlations induced by the cross shell excitations either the spherical normal configuration, or the deformed one, becomes the ground state while the other configuration forms a low lying  $0_2^+$  state. Therefore the discovery and characterization of this  $0_2^+$  state in  $^{44}\text{S}_{28}$  represent crucial information for understanding the evolution of N=28 shell gap. The non spherical nature of the  $^{44}\text{S}$  ground state was suggested by its short  $\beta$  half-life and weak neutron-delayed emission probability [7], by the low energy of the  $2_1^+$  state (1297(18) keV), and the enhanced reduced transition probability  $B(E2 : 2_1^+ \rightarrow 0_1^+)$  of  $63(18) \text{ e}^2\text{fm}^4$  [8]. However the  $2_1^+$  and  $B(E2)$  values are intermediate between a rigid rotor and a spherical nucleus. It suggests a possible mixing of spherical and deformed shapes which can be deduced by studying the properties of the  $0_2^+$  isomer at 1365(1) keV observed in [9]. Already the study of a  $7/2^-$  isomer in  $^{43}\text{S}$  [5, 6] has shed light on shape coexistence in the N $\approx$ 28 region. Other cases of shape coexistence around shell closures have been reported in [10, 11].

The present letter reports on the determination of the monopole strength  $\rho^2(E0 : 0_2^+ \rightarrow 0_1^+)$  and the reduced transition probability  $B(E2 : 2_1^+ \rightarrow 0_2^+)$  in  $^{44}\text{S}$ , extracted from the measurement of the half-life and the branching ratio between the E0 and E2 decay of the isomeric

---

\*Electronic address: grevy@in2p3.fr

$0_2^+$  state. These pieces of information were obtained by using combined  $\gamma$  and electron delayed-spectroscopy and are used to demonstrate the shape coexistence in  $^{44}\text{S}$ .

The experiment was carried out at the Grand Accélérateur National d'Ions Lourds (GANIL) facility. A primary beam of  $^{48}\text{Ca}$  at 60A·MeV ( $I \sim 2e\mu\text{A}$ ) impinged onto a 138 mg/cm<sup>2</sup> Be target to produce neutron-rich fragments. They were separated by the LISE3 spectrometer [12] using an achromatic 100 mg/cm<sup>2</sup> Be degrader. The magnetic rigidity was set to optimize the transmission of the  $^{44}\text{S}$  nuclei, produced at a rate of 200 sec<sup>-1</sup>, with a momentum acceptance of  $\pm 1.45\%$ . Fragments were identified on an event by event basis by means of their energy loss and magnetic rigidity ( $B\rho$ ) values. The  $B\rho$  was obtained from the position of the fragments at the dispersive focal plane given by a multi-wire proportional chamber (CAVIAR) [13]. The selected nuclei were implanted in a 125  $\mu\text{m}$  kapton foil tilted at 20 degrees with respect to the beam axis. Before the foil, a stack of Si detectors, including a position-sensitive one, was used to adjust the implantation depth and to reconstruct the position of the ions in a plane perpendicular to the beam axis. A thick Si detector located downstream to the implantation foil was used as veto. The  $\gamma$  and electron decay events were registered up to 20  $\mu\text{sec}$  after the implantation. Electrons were detected in four cooled 45\*45 mm<sup>2</sup>, 4 mm thick Si(Li) detectors, placed 20 mm above and below the beam axis. The  $\gamma$ -rays were measured by two clover Ge detectors of the EXOGAM array located on the side of the implantation foil, at a distance of 25 mm to the beam axis. The use of a parallel beam optics along 2 meters length enables to derive the ion implantation profile on the kapton foil from the position-sensitive Si detector. This ion profile, the geometry of the detectors and that of the chamber were used as ingredients in a GEANT4 simulation to derive the electron ( $\epsilon_{e^-}$ ) and  $\gamma$  ( $\epsilon_\gamma$ ) efficiencies. The simulated efficiencies compare well with the ones obtained with calibrated sources of  $^{207}\text{Bi}$  and  $^{152}\text{Eu}$  placed in calibration runs at 6 different positions on the implantation foil. Using these comparisons,  $\epsilon_\gamma = 3.06(5)\%$  and  $\epsilon_{e^-} = 13.3(6)\%$  were adopted for a gamma-ray of 1329 keV and an electron of 1362.5 keV, respectively [14].

The decay of the  $0_2^+$  to the ground-state (E0) proceeds through the emission of an internal conversion electron (IC) and by internal pair formation (IPF). The electron spectrum, following the implantation of a  $^{44}\text{S}$  nucleus, is shown in Fig. 1. A single peak is observed at 1362.5(10) keV corresponding to an excitation energy of 1365(1) keV for the  $0_2^+$  state, after having corrected for the binding energy of the K electrons in the  $^{44}\text{S}$  nucleus. The integral of the peak is  $I_{e_{IC}}^-(E0) = 148(8) \times 10^3$ . The low energy part of the spectrum is well accounted for by the pair formation (IPF) mechanism in which electrons and positrons share an energy of  $1365 - (2 \times 511) = 343$  keV. The fit of the electron time distribution (insert of Fig. 1) leads to an half-life of 2.619(26)  $\mu\text{sec}$ , which agrees with the value of 2.3(5)  $\mu\text{sec}$  reported in [9].

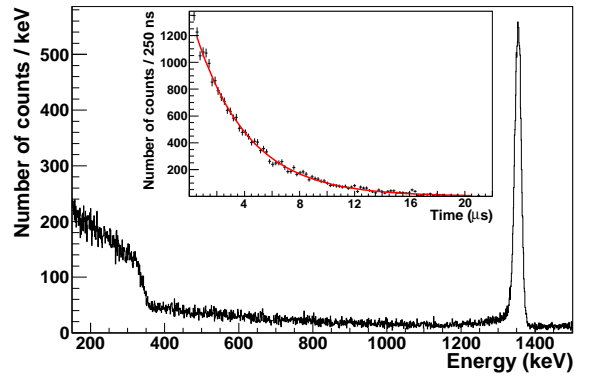


FIG. 1: Electron energy spectrum obtained from the Si(Li) detectors following the implantation of  $^{44}\text{S}$  nuclei. The peak at 1362.5(1.0) keV corresponds to the  $0_2^+ \rightarrow 0_1^+$  E0 transition. The low energy part is due to pair creation. Insert: Time distribution of the 1362.5 keV electron transition from which a half-life of 2.619(26)  $\mu\text{sec}$  is extracted.

The  $0_2^+ \rightarrow 2_1^+$  decay branch, occurs through a strongly converted E2 transition at 36(1) keV, an energy below the experimental threshold of the detection system. The energy of this unobserved transition is derived from the measured energies of the  $0_2^+$  and  $2_1^+$  states, the latter being obtained from the observation of a delayed  $2_1^+ \rightarrow 0_1^+$  transition at 1329.0(5) keV (half-life of 2.66(23)  $\mu\text{sec}$ , in agreement with the value obtained from the electron spectrum) which follows the  $0_2^+ \rightarrow 2_1^+$  decay. The 1329 keV energy agrees with the value of 1297(18) found in Ref. [8]. The yield of the  $0_2^+ \rightarrow 2_1^+$  transition,  $I_\gamma(E2)$ , has been extracted from the number of delayed  $2_1^+ \rightarrow 0_1^+$   $\gamma$ -rays. As can be seen in the insert of Fig. 2, this transition is contaminated by the 1332.5 keV  $\gamma$ -ray of  $^{60}\text{Co}$  arising from the activation of the last selection slits of the spectrometer, which also produce a 1173 keV  $\gamma$ -ray with the same intensity. The number of counts in the 1329 keV peak has been obtained by fitting the  $\gamma$  spectrum with two gaussians, the intensity of the 1332.5 keV transition being constrained by that of the 1173 keV  $\gamma$ -ray. The resulting  $I_\gamma(E2)$  is  $56(3) \times 10^3$ .

The decay of the  $0_2^+$  state occurs through E2 and E0 transitions, the ratio of which is expressed as :

$$R = \frac{\lambda(E2)}{\lambda(E0)} = \frac{I_\gamma(E2)}{I_{e_{IC}}^-(E0)} \frac{1 + \alpha_{conv}(2_1^+ \rightarrow 0_1^+)}{1 + \frac{\Omega_{IPF}}{\Omega_{IC}}} \quad (1)$$

In this expression, the electronic factors for pair formation and internal conversion have been extrapolated for a nucleus with  $A=44$  from Ref. [15–17] to be  $\Omega_{IPF} = 1.495 \times 10^7 \text{sec}^{-1}$  and  $\Omega_{IC} = 1.1125 \times 10^7 \text{sec}^{-1}$ , respectively. A value of  $3.6 \times 10^{-5}$  has been taken for the conversion coefficient  $\alpha_{conv}(2_1^+ \rightarrow 0_1^+)$  [18]. Using the experimental values of electron  $I_{e_{IC}}^-(E0)$  and  $\gamma$ -ray  $I_\gamma(E2)$  yields derived above, the resulting branching ratio is  $R = 0.163(13)$ . The  $\rho^2(E0 : 0_2^+ \rightarrow 0_1^+)$  and  $B(E2 : 2_1^+ \rightarrow 0_2^+)$

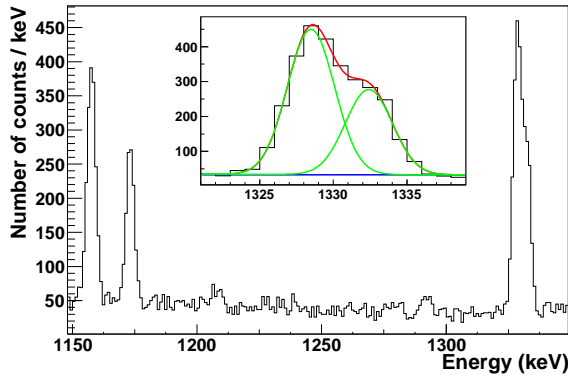


FIG. 2: Part of the delayed gamma energy spectrum following the implantation of  $^{44}\text{S}$  nuclei. Peaks from the  $\beta$  decay of  $^{44}\text{K}$  (1158 keV) and  $^{60}\text{Co}$  (1173 and 1332.5 keV) are identified, the latter overlapping with the 1329 keV  $2_1^+ \rightarrow 0_1^+$  transition of  $^{44}\text{S}$ . The deconvolution of this doublet is shown in the insert.

values are obtained using the following equations :

$$\rho^2(E0) = \frac{\ln(2)}{T_{1/2}(0_2^+)(1+R)(\Omega_{IPF} + \Omega_{IC})} \quad (2)$$

$$B(E2) = \frac{5.65 \times 10^{-10}}{5E_\gamma^5 T_{1/2} (1 + \frac{1}{R})(1 + \alpha_{conv}(0_2^+ \rightarrow 2_1^+))} \quad (3)$$

Using the measured branching ratio  $R$ , the half-life value  $T_{1/2}(0_2^+)$  and  $\alpha_{conv}(0_2^+ \rightarrow 2_1^+) = 10.94(1)$  extrapolated from Ref. [18], the monopole strength  $\rho^2(E0 : 0_2^+ \rightarrow 0_1^+)$  and the reduced transition probability  $B(E2 : 2_1^+ \rightarrow 0_2^+)$  have been determined to be  $8.7(7) \times 10^{-3}$  and  $8.4(26) \text{ e}^2 \text{ fm}^4$ , respectively.

The values of  $E(0_2^+) = 1365(1) \text{ keV}$  and  $\rho^2(E0) = 8.7(7) \times 10^{-3}$  are the smallest measured in this mass region, pointing to a weak mixing between the  $0_1^+$  ground state and the  $0_2^+$  isomer and therefore to shape coexistence. In case of a large mixing, these states would repel each other to exhibit a large energy spacing and a larger  $\rho^2(E0)$  value. To obtain further understanding on the nature of the shape coexistence, data are compared to shell model calculations.

Shell model (SM) calculations have been performed for  $^{44}_{16}\text{S}_{28}$  using the ANTOINE code [19] and the up-to-date SDPF-U interaction that accounts remarkably well for nuclear structure in this mass region [20]. The full  $sd$  ( $fp$ ) valence space has been considered for protons (neutrons) using standard effective charges  $e_\pi = 1.35 e$  ( $e_\nu = 0.35 e$ ).

The results gathered in Table I show a good agreement with the experimental values, the only exception is a somewhat larger calculated  $B(E2 : 2_1^+ \rightarrow 0_2^+)$  value than measured. Nevertheless, both experiment and calculation agree with the fact that the  $2_1^+$  state connects much strongly with the  $0_1^+$  state than with the  $0_2^+$  one. Indeed, the experimental  $B(E2 : 2_1^+ \rightarrow 0_1^+)/B(E2 : 2_1^+ \rightarrow 0_2^+)$  ratio is 7.5 whereas the calculated one is 3.2. Calculated excited states connected to these two  $0^+$  states are presented in Fig. 3 with their intrinsic quadrupole moments

TABLE I: Experimental and shell model values for the excitation energies, in MeV, and reduced transition probabilities  $B(E2)$ , in  $\text{e}^2 \text{ fm}^4$ , of  $^{44}\text{S}$ .

$E/B(E2)$	$2_1^+$	$0_2^+$	$2_2^+$	$2_1^+ \rightarrow 0_1^+$	$2_1^+ \rightarrow 0_2^+$
exp.	1.329(1)	1.365(1)	2.335(39)	63(18)	8.4(26)
SM	1.172	1.137	2.140	75	19

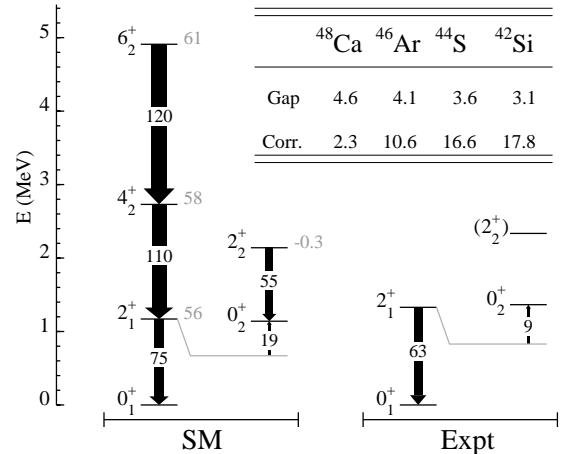


FIG. 3:  $^{44}\text{S}$  level scheme calculated within the present SM approach (left), compared with available experimental data (right).  $E2$  transition probabilities (in  $\text{e}^2 \text{ fm}^4$ ) are reported on top of black arrows and intrinsic quadrupole moments (in  $\text{efm}^2$ ) are shown in light gray on the right side of calculated levels. The ground state of the nucleus is head of a rotational band ( $\beta \simeq 0.25$ ) and coexists with the rather spherical low-lying  $0_2^+$  isomer. Calculated values of the  $N=28$  gap and correlation energies (in MeV) are given for even-even  $N=28$  isotones.

$Q_0$ . For sake of clarity only the states of present interest are shown in this picture. Remarkable is the presence of  $2_1^+$ ,  $4_2^+$  and  $6_2^+$  states on top of the  $0_1^+$  ground state connected by large  $B(E2)$  values. These states present equal  $Q_0$  values of about  $60 \text{ efm}^2$ . These two features characterize the presence of a rotational band from an axially deformed nucleus with  $\beta \simeq 0.25$ . The  $2_2^+$  state at 2.14 MeV has a smaller intrinsic quadrupole moment  $Q_0 = -0.3 \text{ efm}^2$  compatible with a spherical shape. A candidate for the  $2_2^+$  state is proposed at 2335(39) keV by placing the previously reported 988 keV transition [21] on top of the  $0_2^+$  or  $2_1^+$  state. Hence SM calculations suggest a prolate-spherical shape coexistence in  $^{44}\text{S}$ .

A detailed analysis of the components contributing to the total energy of the  $0^+$  states has been performed in order to deepen our understanding on the evolution of the collectivity from  $^{48}_{20}\text{Ca}$  to  $^{42}_{14}\text{Si}$ . Within the SM framework, the total Hamiltonian can be separated into its monopole (i.e. spherical mean-field contribution) and multipole (i.e. correlations mainly of pairing and quadrupole type) parts [22]. As can be seen from the values reported in Fig. 3, correlations strongly increase from the dou-

bly magic  $^{48}\text{Ca}$  ( $\simeq 2$  MeV) down to the exotic deformed  $^{42}\text{Si}$  ( $\simeq 18$  MeV), while the size of the N=28 shell gap gets slightly reduced [23]. This increase of correlations is favored on one hand by neutron quadrupole excitations across the N=28 gap between the  $f_{7/2}$  and  $p_{3/2}$  orbits [23], and on the other hand, by the degeneracy of proton  $s_{1/2}$  and  $d_{3/2}$  orbits and excitations from the  $d_{5/2}$  shell [1, 24–26]. In both cases, quadrupole correlations are favored by the fact that occupied and valence states are separated by two units of angular momentum. Without considering multipole contributions to the  $0_1^+$  and  $0_2^+$  states in  $^{44}\text{S}$ , both levels are found to be quasi-degenerate in energy, and the ground state of  $^{44}\text{S}$  is spherical. A gain of 1.5 MeV from the multipole energy brings the deformed configuration at the minimum of binding energy, while the spherical configuration corresponds to the excited state. Similar multipole effects energetically favor the oblate  $0^+$  state in  $^{42}\text{Si}$  which is predicted to coexist with a prolate  $0^+$  state [20] at 1293 keV.

The shell model calculation uses an Harmonic Oscillator basis for the description of the atomic nucleus. From the definition of the E0 operator, the calculated E0 transition between states of the same harmonic oscillator shells, as for protons in the  $sd$  shells and neutron in the  $fp$  shells, is strictly zero. Therefore, in order to shed light on the amount of mixing between the  $0_{1,2}^+$  states and to deduce their shape before mixing, we use a phenomenological two interacting levels model. We assume two spherical (S) and deformed (D) states before mixing which interact to produce  $0_1^+$  and  $0_2^+$  states defined as :

$$|0_1\rangle = \cos\theta|0_D\rangle + \sin\theta|0_S\rangle \quad (4)$$

$$|0_2\rangle = -\sin\theta|0_D\rangle + \cos\theta|0_S\rangle \quad (5)$$

where  $\theta$  is the mixing angle. The E2 transition between the  $2_1^+$  and  $0_2^+$  (or  $0_1^+$ ) states being mainly due to the D-component of these  $0^+$  states, it follows that  $B(\text{E}2 : 2_1^+ \rightarrow 0_2^+)/B(\text{E}2 : 2_1^+ \rightarrow 0_1^+) \sim \tan^2(\theta)$  (eq. 2 of [27]). A mixing amplitude  $\tan^2(\theta)=0.13$  is deduced from the

experimental B(E2) values whereas the shell model gives a somewhat larger value of 0.24, both being smaller than the case of a maximum mixing ( $\tan^2(\theta)=1$ ). Therefore, the shape coexistence is found to be more pronounced experimentally than calculated by the SM. The magnitude of the monopole matrix element can be written as a function of the mixing amplitude and of the difference of shapes,  $\beta_S$  and  $\beta_D$ , between the two configurations before mixing [28],  $\rho^2(E0)=(3Ze/4\pi)^2 \sin^2\theta \cos^2\theta (\beta_D^2 - \beta_S^2)^2$ . Using the experimental mixing amplitude value of  $\tan^2(\theta)$  in this equation, the experimental monopole strength is reproduced only when deformations  $\beta_D \simeq 0.274$  and  $\beta_S=0$  are assumed. The deformation parameter  $\beta_D$  is in close agreement with the values obtained after mixing from Coulomb excitation experiment [8],  $\beta = 0.258(36)$ , and from the shell model calculations,  $\beta=0.25$ . Altogether these values again point towards a deformed-spherical shape coexistence in  $^{44}\text{S}$ .

To summarize, electron and  $\gamma$  delayed-spectroscopies have been used to determine the monopole strength  $\rho^2(E0 : 0_2^+ \rightarrow 0_1^+)=8.7(7)\times 10^{-3}$  and the reduced transition probability  $B(\text{E}2 : 2_1^+ \rightarrow 0_2^+)=8.4(26) \text{ e}^2\text{fm}^4$  in the  $^{44}_{16}\text{S}_{28}$  nucleus. Using these values, the earlier measured  $B(\text{E}2 : 2_1^+ \rightarrow 0_1^+)$  [8], shell model calculations and a two level mixing model, it is found that  $^{44}\text{S}$  exhibit a shape coexistence between a prolate ground state ( $\beta \simeq 0.25$ ) and a rather spherical  $0_2^+$  state. This establishes how the onset of collectivity progressively develops between the spherical  $^{48}_{20}\text{Ca}$  and the deformed  $^{42}_{14}\text{Si}$  nuclei. This study completes uniquely the understanding of the shell-breaking mechanism at the spin-orbit closed-shell N=28, which is as well of importance for the evolution of other shell gaps having the same origin.

We are grateful to the GANIL staff and the LISE team for support. We acknowledge P. Van Isaker for fruitful discussions. This work was supported by CNCSIS-UEFISCSU, proj. numb. PNII-IDEI 933/2007, Academy of Sciences of Czech Rep. and by the European Community through OTKA K68801.

- 
- [1] B. Bastin *et al.*, Phys. Rev. Lett. **99**, 022503(2007)  
[2] T. R. Werner *et al.*, Nucl. Phys. **A597**, 327(1996); P.-G. Reinhardt *et al.*, Phys. Rev. **C60**, 014316(1999) ; G.A. Lalazissis *et al.*, Phys. Rev. **C 60** (1999) 014310 ; R. Rodriguez-Guzman *et al.*, Phys. Rev. **C65**, 024304(2002)  
[3] S. Péru, M. Girod, and J.F. Berger, Eur. Phys. J. A **9**, 35 (2000)  
[4] E. Caurier, F. Nowacki and A. Poves, Nucl. Phys. **A742**, 14(2004)  
[5] F. Sarazin *et al.*, Phys. Rev. Lett. **84**, 5062(2000)  
[6] L. Gaudefroy *et al.*, Phys. Rev. Lett. **102**, 092501(2009)  
[7] O. Sorlin *et al.*, Phys. Rev. **C47**, 2941(1993)  
[8] T. Glasmacher *et al.*, Phys. Lett. **B395**, 163(1997)  
[9] S. Grévy *et al.*, Eur. Phys. J. **A25**, s01-111(2005)  
[10] S. Shimoura *et al.*, Phys. Lett. **B560**, 31(2003); S. Shimoura *et al.*, Phys. Lett. **B654**, 87(2007)  
[11] W. Schwerdtfeger *et al.*, Phys. Rev. Lett. **103**, 012501 (2009)  
[12] R. Anne *et al.*, Nucl. Instr. and Meth. **A257**, 215(1987)  
[13] L. Perrot *et al.*, 11<sup>th</sup> Int. Conf. on HEAVY ION ACCELERATOR TECHNOLOGY, Venice Italy, 2009.  
[14] [http://tel.archives-ouvertes.fr/docs/00/43/01/25/PDF/Manuscrit\\_These\\_final.pdf](http://tel.archives-ouvertes.fr/docs/00/43/01/25/PDF/Manuscrit_These_final.pdf)  
[15] A. Passoja and T. Salonen, report JYFL RR-2/86 (1986)  
[16] E. L. Church and J. Weneser, Phys. Rev. **103**, 1035(1956)  
[17] D. H. Wilkinson *et al.*, Nucl. Phys. **A133**, 1(1969)  
[18] I. M. Band *et al.*, At. Data Nucl. Data Tables **18**, 433(1976)  
[19] E. Caurier *et al.*, Rev. Mod. Phys. **77**, 427 (2005)  
[20] F. Nowacki and A. Poves, Phys. Rev. **C79**, 014310(2009)  
[21] D. Sohler *et al.*, Phys. Rev. **C66**, 054302(2002)  
[22] M. Dufour and A. P. Zuker, Phys. Rev. **C 54**, 1641 (1996).  
[23] L. Gaudefroy *et al.*, Phys. Rev. Lett. **99**, 099202 (2007).

[24] L. A. Riley *et al*, Phys. Rev. C **78**, 011303(2008)  
[25] L. Gaudefroy, Phys. Rev. C **81**, 064329 (2010).  
[26] M. De Rydt *et al*, Phys. Rev. C **81**, 034308 (2010).

[27] H. Mach *et al.*, Phys. Lett. B **230**, 21(1989)  
[28] J. L. Wood *et al.*, Nucl. Phys. A **651**, 323(1999)